ACTIVITY REPORT 2015

Project no. 290/05.11.2011

Within the actual stage we have continued with (i) the study of up-conversion effects shown by (Yb^{3+}-Er^{3+}) doped SiO_2-$YLiF_4$ glass-ceramics nanorods and (ii) we have prepared Ho^{3+}-doped SiO_2-$YLiF_4$ glass-ceramics nanorods.

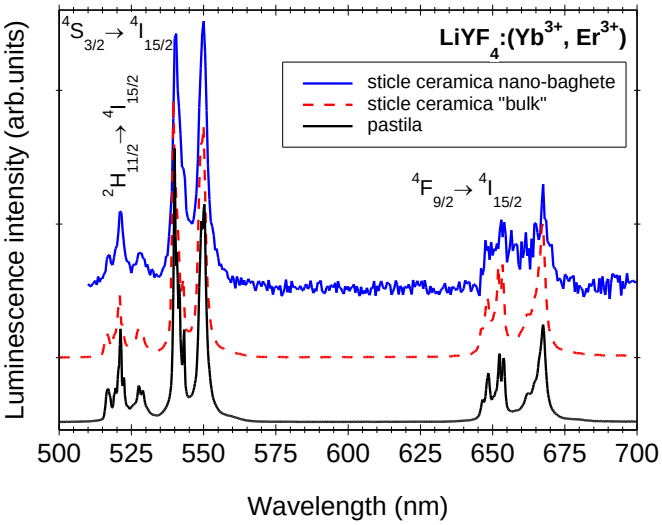

Figure 1. Green ($^2H_{11/2}$, $^4S_{3/2}$ → $^4I_{15/2}$) and red ($^4F_{9/2}$ → $^4I_{15/2}$) Er^{3+} up-conversion luminescences excited at 980 nm in Yb^{3+}-Er^{3+}-doped oxyfluoride glass-ceramic „bulk" or nanorods and $LiYF_4$ pellet samples.

Up-conversion properties of Yb^{3+}/Er^{3+} co-doped $LiYF_4$ nanocrystals in glass-ceramics „bulk" or nanorods have been studied by comparison to the corresponding glass-ceramic. Under 980 nm laser light pumping the green emitting levels ($^2H_{11/2}$, $^4S_{3/2}$) are populated by the Yb^{3+} - Er^{3+} ET1 [$^2F_{5/2}$ (Yb^{3+}) + $^4I_{15/2}$ (Er^{3+}) →$^2F_{7/2}$ (Yb^{3+}) + $^4I_{11/2}$ (Er^{3+})] and ET2 [$^2F_{5/2}$ (Yb^{3+}) + $^4I_{11/2}$ (Er^{3+}) →$^2F_{7/2}$ (Yb^{3+}) + $^4F_{7/2}$ (Er^{3+})] processes (Figures 1-2), followed by the rapid multiphonon (MP) transition $^4F_{7/2}$ → $^2H_{11/2}$. The lower emitting levels are then populated via multiphonon and cross-relaxation (Yb^{3+}-Er^{3+}) processes followed by the green (($^2H_{11/2}$, $^4S_{3/2}$) → $^4I_{15/2}$) and red ($^4F_{9/2}$ → $^4I_{15/2}$) luminescences.

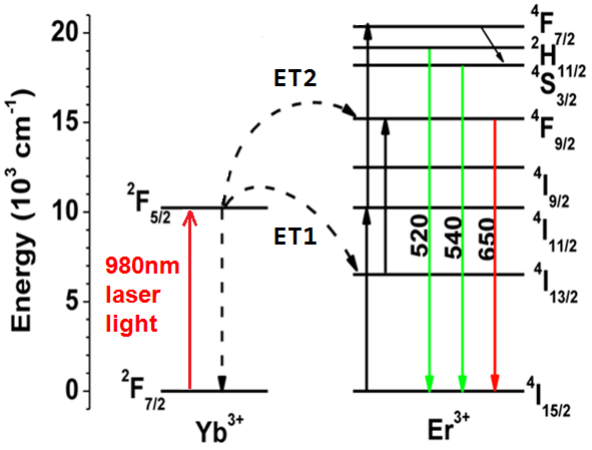

Figure 2. Energy level schemes of Yb^{3+} and Er^{3+} and the main energy transfer processes from Yb^{3+} to Er^{3+} represented by curved dashed arrows.

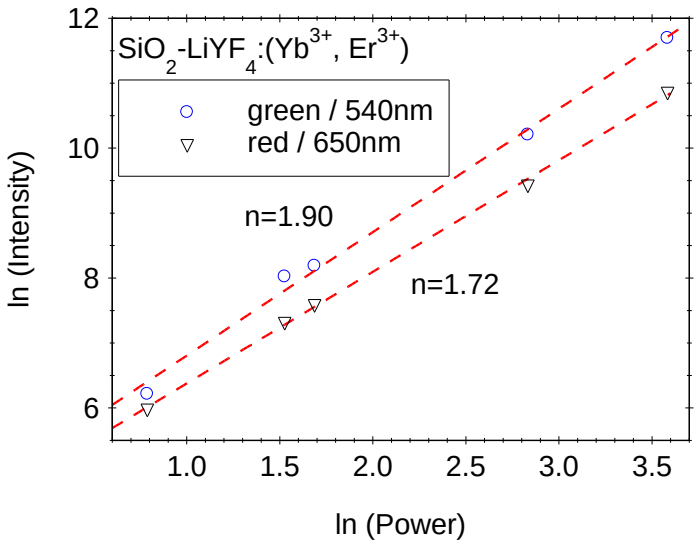

Figure 3. Double logarithmic plot of luminescence intensity vs. incident laser power for green (($^2H_{11/2}$, $^4S_{3/2}$) → $^4I_{15/2}$) and red ($^4F_{9/2}$ → $^4I_{15/2}$) luminescences recorded on Yb^{3+}/Er^{3+} co-doped $LiYF_4$ glass ceramic „bulk" (or nanorods) and $LiYF_4$ pellet samples.

Laser pump power dependencies of UC luminescence intensities show a quadratic laser power dependence indicating a two-photon process (Figure 3). Photoluminescence lifetimes measurements have shown a drastically reduction of the 540nm „green" luminescence decay time from 0.015±0.001 ms in the glass ceramic bulk to to about 0.001ms in the naorods that indicates the influence of the dimensional constraints imposed by the membrane pores during xerogel formation and glass ceramization.

Preparation of the Ho-doped glass-ceramics nanorods was made by using the template method and nanoporous polycarbonate membranes (pore diameter size 800nm). The method implies the filling of the pores of the membrane and nanorods/nanowires followed solidification and membrane separation by dissolving. RE-doped gels ($95SiO_2$–$5LiYF_4$) (mol%) doped with rare earths Yb (4mol% mol.) and Ho(1% mol) have been prepared by using tetraethylorthosilicate (TEOS) as precursor and trifluoroacetic acid (TFA) as fluorine agent; Yb and Ho acetates have been used for doping. For the first solution that imply (TEOS-tetraethoxysilane) precursor liquid we used two different molar ratio for the ethanol to water: TEOS:Et:H2O:CH3COOH is 1 : **10 : 4** : 0.5 **(A synthesis)** si TEOS:Et:H2O:CH3COOH is 1 : **4 : 10** : 0.5 **(B synthesis).** For the glass ceramization we have used a thermal tratement at higher temperatures. Crystallization mechanism involves the formation of the nucleating centres due to the thermolysis (thermal decomposition) of the $Y(CF_3COO)_3$ $Li(CF_3COO)$ acetates with the formation of YF_3 and LiF, followed at higher temperatures (530 ^oC) by the $LiYF_4$ nanocrystals formation with the Ho si Yb dopants incorporation (Figure 4).

Morphological and structural characterisation of the glass-ceramics nanorods has been made by using X-ray difraction (XRD) and scanning electron microscopy (SEM) measurements. The small quantities of the material (glass ceramic rods) and sensitivity of the x-ray diffraction technique (of about 2-3%) did not allow to measure the $LiYF_4$ crystallized fraction within the rods and therefore these studies have been performed on "bulk"(powder samples) based on the supposition that the crystallization processes are the same within the "bulk" and rods. The

XRD pattern of the glass ceramics „bulk" has shown diffraction peaks due to the $LiYF_4$ crystalline phase precipitation in the glass matrix. From the analysis of the XRD pattern we have extracted the mean size of the nanocrystals which is d≅ 55-60nm (A synthesis) and d≅ 25-30nm (B synthesis). On the other hand the crystallization fraction is about 40% for the A synthesis and only 20% for the B synthesis. SEM images have shown that in the first case the nanorods are partially agglomerated and are curved or bent; in both cases are formed $LiYF_4$ nanocryslas as the UP-conversion luminescence spectra have shown.

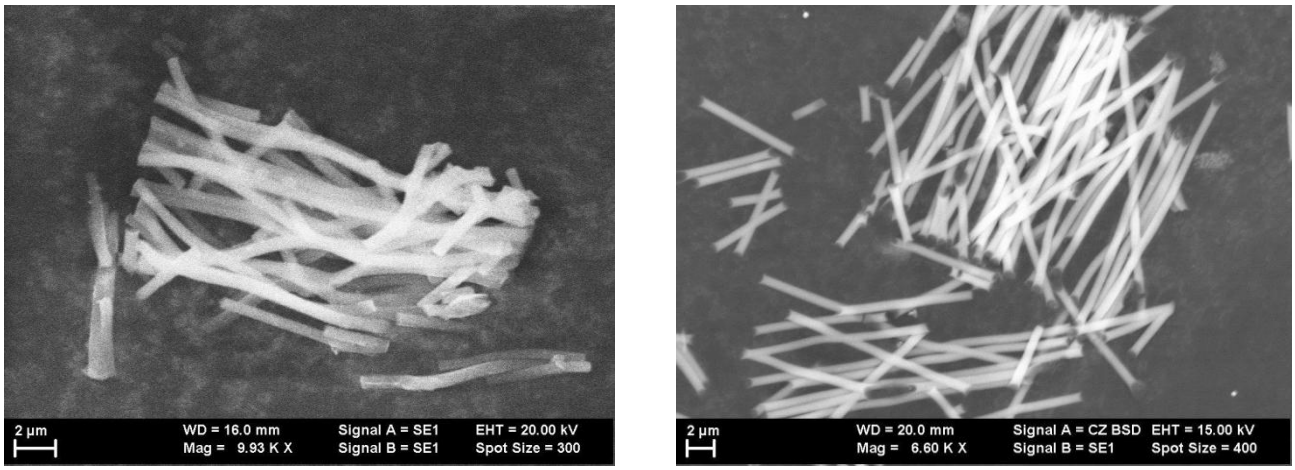

Figure 4. SEM images of the oxyfluoride glass-ceramic SiO2-LiYF4(Yb,RE) microrods.

In conclusion, up-conversion properties of Yb^{3+}/Er^{3+} co-doped $LiYF_4$ nanocrystals are similar in the glass-ceramics („bulk" or nanorods) and pellet showing green (($^2H_{11/2}$, $^4S_{3/2}$) → $^4I_{15/2}$) and red ($^4F_{9/2}$ → $^4I_{15/2}$) up-conversion luminescence bands due to the Er^{3+} ions. Laser pump power dependencies of UC showed a quadratic laser power dependence indicating a two-photon process. The non-radiatie decay processes are much higher in the glass ceramic rods compared to the bulk an effect that might be related to the quasi-unidimensional morphology of the nanorods.

Regarding the synthesis of the Ho^{3+} doped YLF ($YLiF_4$) nanorods it was shown that the molar ratio ethanol/water has a great influence on the crystallization fraction but weaker on the nanocrystals size.

References:

1. *„Up-conversion luminescence of Er^{3+}/Yb^{3+} co-doped $LiYF_4$ nanocrystals in sol-gel derived oxyfluoride glass-ceramics"* M. Secu and C.E. Secu Journal of Non-Crystalline Solids 426 (2015) 78–82

2. *„Luminescence properties of Eu^{3+}-doped SiO_2–$LiYF_4$ glass–ceramic microrods"*

C.E. Secu and M. Secu Optical Materials 47 (2015) 95–98

Director proiect,

Dr. Mihail SECU